

# Comparative study of creep of cast Ti-46Al-2W-0.5Si and Ti-45Al-2W-0.6Si-0.7B alloys

J. Lapin\*

*Institute of Materials and Machine Mechanics, Slovak Academy of Sciences, Račianska 75, 831 02 Bratislava, Slovak Republic*

Received 2 November 2005, accepted 14 November 2005

## Abstract

Creep properties of two cast TiAl-based alloys with nominal chemical composition Ti-46Al-2W-0.5Si and Ti-45Al-2W-0.6Si-0.7B (in at.%) were investigated. The constant load creep tests were performed in air at applied stresses ranging from 200 to 390 MPa in the temperature range from 973 to 1073 K. For both alloys, the minimum creep rate is found to depend strongly on the applied stress and temperature. The power law stress exponents of minimum creep rate and the apparent activation energies for creep are determined. The initial microstructure of the alloys is unstable. In the lamellar and feathery regions, the  $\alpha_2$ (Ti<sub>3</sub>Al)-phase transforms to the  $\gamma$ (TiAl)-phase, B2 particles and fine Ti<sub>5</sub>Si<sub>3</sub> precipitates. The main microstructural change observed in the  $\gamma$ -rich region was precipitation of fine Ti<sub>5</sub>Si<sub>3</sub> particles. Ordinary dislocations in the  $\gamma$  matrix dominate the deformation microstructures at creep strains lower than 1.5 %. For both alloys at low creep strains, the kinetics of the creep deformation is proposed to be controlled by non-conservative motion of dislocations. The alloy doped by boron shows superior creep resistance when compared to that of boron-free counterpart alloy.

**Key words:** titanium aluminides, TiAl, creep properties, microstructure

## 1. Introduction

TiAl-based intermetallic alloys have been extensively studied as potential high-temperature structural materials in the gas turbine and automotive industry for various applications such as blades in the last stage of the low-pressure turbine, high-pressure compressor blades, vanes, casings, diffusers, automotive exhaust valves and turbocharger wheels [1–6]. At intermediate temperatures (about 1023 K), these alloys can successfully compete with titanium alloys [7], nickel based single crystalline superalloys [8–10], nickel aluminides [11–14], or iron aluminides [15–17]. Since TiAl-based alloys are difficult to hot work, cold work or machine, large attention is paid to investment cast alloys [18].

Among various TiAl-based systems, cast ABB-2 and ABB-23 alloys with nominal chemical composition Ti-46Al-2W-0.5Si and Ti-45Al-2W-0.6Si-0.7B (in at.%), respectively, have been developed as potential blade material for stationary gas turbines

[4]. The ABB-23 alloy was derived from its boron-free counterpart ABB-2 alloy [19]. Alloying by boron was proved to be an effective and economic method to achieve grain refinement, reduce lamellar colony size and prevent uncontrolled grain growth during heat treatments performed within the single phase  $\alpha$ -field [20–22]. In spite of the fact that the microstructure, microstructure stability and creep behaviour of the ABB-2 and ABB-23 alloys have been studied by several authors [23–27], microstructure stability and mechanical properties of small simple shape specimens can differ significantly from those prepared from large complex shape castings. Therefore, it is of great importance to study microstructural and mechanical properties on prototype castings and to define real application potential of these alloys for the industry.

The aim of this paper is to study creep properties of two investment cast alloys with nominal chemical composition Ti-46Al-2W-0.5Si and Ti-45Al-2W-0.6Si-0.7B (in at.%). The initial microstructure, micro-

---

\*Tel.: +421 2 49268290; fax: +421 2 44253301; e-mail address: ummslapi@savba.sk

structure stability, deformation microstructures and kinetics of creep deformation are reported and discussed.

## 2. Experimental procedure

Creep experiments were conducted on the alloys with the chemical compositions given in Table 1. The material was provided by Alstom Ltd. in the form of large investment cast turbine blades, plate with dimensions  $15 \times 75 \times 121$  mm and cast cylindrical bars with diameter of 16 mm and length of 200 mm. The as-received components were subjected to hot isostatic pressing at applied pressure of 172 MPa and temperature of 1533 or 1543 K (Blade 2) for 4 h, which was followed by solution annealing at 1623 K for 1 h and gas fan cooling. The heat treatment was completed by stabilization annealing at 1273 K for 6 h and furnace cooling to room temperature.

Tensile creep specimens with a gauge length of 20 mm and gauge diameter of 4 mm were cut from the central part of the cast components by electro spark machining. After lathe machining, the specimen surface was polished to a roughness of about  $0.3 \mu\text{m}$ . Constant load creep tests in air were performed at temperatures of 973, 1023, and 1073 K under initial tensile stresses ranging from 200 to 390 MPa. The specimen displacement was measured using a high-temperature extensometer attached to the ledges of the creep specimen. The extensometer was equipped with a linear variable displacement transformer (LVDT). The acquisition of time-elongation data was accomplished by computer and data processing was performed by computer program.

Microstructural analysis was performed by optical microscopy (OM), scanning electron microscopy (SEM), transmission electron microscopy (TEM) and energy dispersive X-ray (EDX) spectroscopy. OM and SEM samples were prepared using standard metallographic techniques and etched in a reagent of 150 ml  $\text{H}_2\text{O}$ , 25 ml  $\text{HNO}_3$  and 10 ml HF. TEM samples were thinned mechanically to thickness of about  $40 \mu\text{m}$  and then by ion milling until perforation. Volume fraction and size of coexisting phases were determined by computerized image analysis.

## 3. Results and discussion

### 3.1. Microstructure before creep

Figure 1a shows the typical as-received microstructure of the ABB-2 alloy. The microstructure of gauge region of creep specimens is equiaxed with an average grain size of about  $600 \mu\text{m}$ . The microstructure within the grains consists of lamellar (66 vol.%),

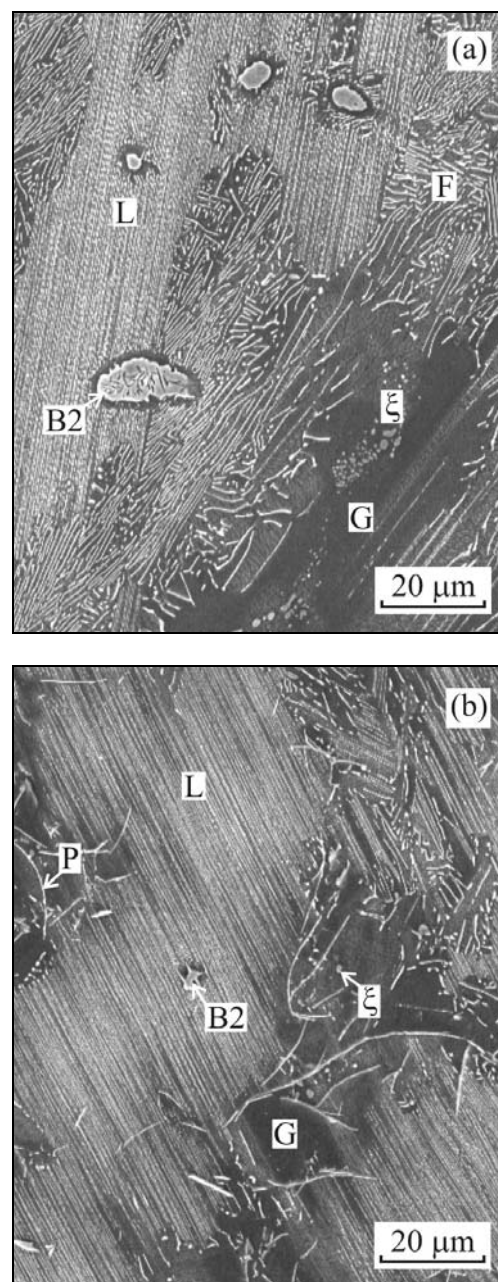


Fig. 1. SEM micrograph showing the typical microstructures in the gauge region of creep specimens before testing: (a) ABB-2 alloy, (b) ABB-23 alloy. L – lamellar region, F – feathery region, G –  $\gamma$ -rich region,  $\xi$  –  $\text{Ti}_5\text{Si}_3$  precipitates, P – boride particles.

feathery (26 vol.%) and  $\gamma$ -rich (8 vol.%) regions. The lamellar regions contain continuous  $\alpha_2(\text{Ti}_3\text{Al})$  lamellae in the  $\gamma(\text{TiAl})$  matrix with a mean  $\alpha_2$ - $\alpha_2$  interlamellar spacing of 645 nm. Besides the continuous lamellae, discontinuous lamellae composed of  $\alpha_2$  segments, fine needle-like B2 particles and  $\text{Ti}_5\text{Si}_3$  precipitates are also observed in the lamellar regions [23, 26]. Some lamellar regions contain coarse blocky type B2 particles. The feathery regions are composed of the

Table 1. Chemical composition of the investment cast components (in at.%)

Material	Ti	Al	W	Si	B	C	Fe	Cu	O	N	H
ABB-2 Plate	Bal.	46.11	2.02	0.48	–	0.017	0.017	0.001	0.168	0.093	0.040
ABB-2 Blade 1	Bal.	46.88	1.96	0.53	–	0.024	0.041	0.004	0.193	0.032	0.040
ABB-2 Blade 2	Bal.	46.23	2.00	0.48	–	0.017	0.015	0.001	0.087	0.038	0.081
ABB-23 Bars	Bal.	45.11	2.01	0.59	0.74	0.020	0.031	0.001	0.184	0.031	0.009

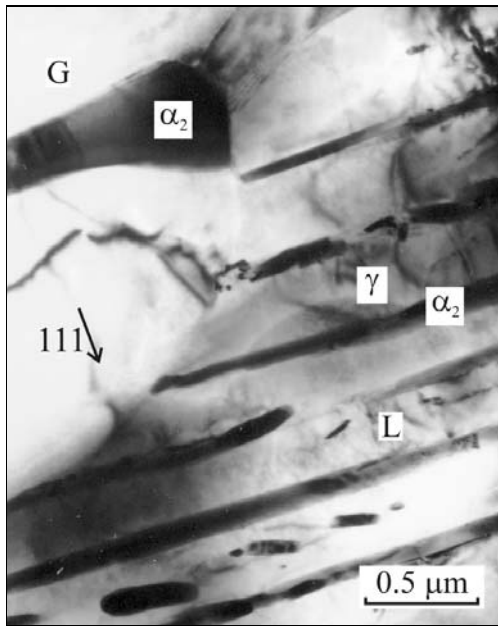


Fig. 2. TEM micrograph showing  $\alpha_2$  lamellae and  $\gamma$  matrix with low dislocation density in lamellar and  $\gamma$ -rich regions of the ABB-23 alloy before creep testing. Zone axis near  $[1\bar{1}0]$  and  $g$  vector  $(111)$ .

$\gamma$  phase, irregular partially decomposed  $\alpha_2$  lamellae, B2 particles and  $\text{Ti}_5\text{Si}_3$  precipitates [23, 26]. The  $\gamma$ -rich regions are composed of the  $\gamma$  matrix and coarse spherical  $\text{Ti}_5\text{Si}_3$  precipitates. Figure 1b shows the typical microstructure of the ABB-23 alloy. The microstructure is equiaxed with an average grain size of 85  $\mu\text{m}$ . The microstructure consists of lamellar regions L (48 vol.%) with an average colony size of 70  $\mu\text{m}$  and elongated  $\gamma$ -rich regions G (52 vol.%). The lamellar regions are composed of  $\alpha_2$  and  $\gamma$  lamellae with a mean  $\alpha_2$ - $\alpha_2$  inter-lamellar spacing of 530 nm. Besides the continuous  $\alpha_2$ -lamellae, lamellae partially decomposed into the  $\gamma$  matrix and needle-like B2 particles are observed. Fine  $\text{Ti}_5\text{Si}_3$  precipitates were identified at lamellar  $\alpha_2/\gamma$  interfaces [22, 28]. Some lamellar regions contain coarse blocky type B2 particles. The  $\gamma$ -rich regions contain  $\gamma$  matrix with numerous ribbon-like boride particles, rod-like B2 particles,  $\alpha_2$  phase and coarse  $\text{Ti}_5\text{Si}_3$  particles. It should be noted that

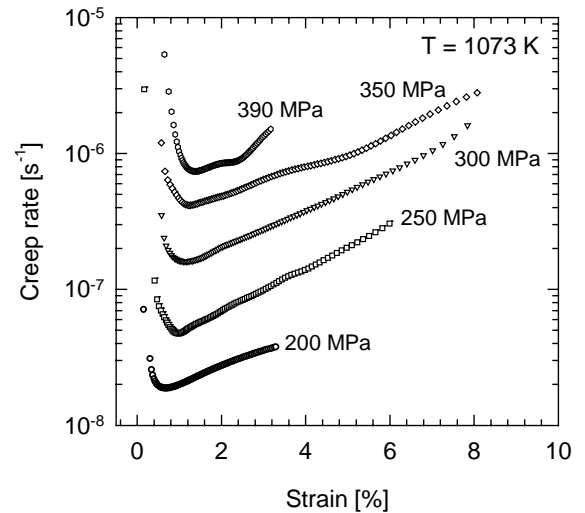


Fig. 3. Dependence of creep rate on the strain for the ABB-23 alloy at 1073 K. The applied stresses are indicated in the figure.

both alloys showed very low dislocation density before creep testing, as illustrated in Fig. 2.

### 3.2. Creep

Figure 3 shows variation of the instantaneous creep rate with the strain. During the primary creep stage the creep rate decreases with increasing strain. After reaching its minimum at a strain of about 1 %, the creep rate continuously increases with increasing strain. Such deformation behaviour is typical for both studied alloys at all testing temperatures and applied stresses. The minimum creep rates  $\dot{\epsilon}_{\text{min}}$  and the applied stresses  $\sigma$  were fitted to the power law

$$\dot{\epsilon}_{\text{min}} = A\sigma^n, \tag{1}$$

where  $A$  is a constant and  $n$  is the stress exponent. Figure 4 shows variation of the minimum creep rate with the applied stress. Using linear regression analysis of the creep data, the stress exponents are determined to vary from 7.1 to 7.6 and from 4.8 to 5.3 for the ABB-2 (Blade 1) and ABB-23 (Bars) alloy, respectively. The correlation coefficients  $r^2$  of these fits are better than 0.96. The measured stress exponents are comparable with those ranging from about 2 at low stresses to

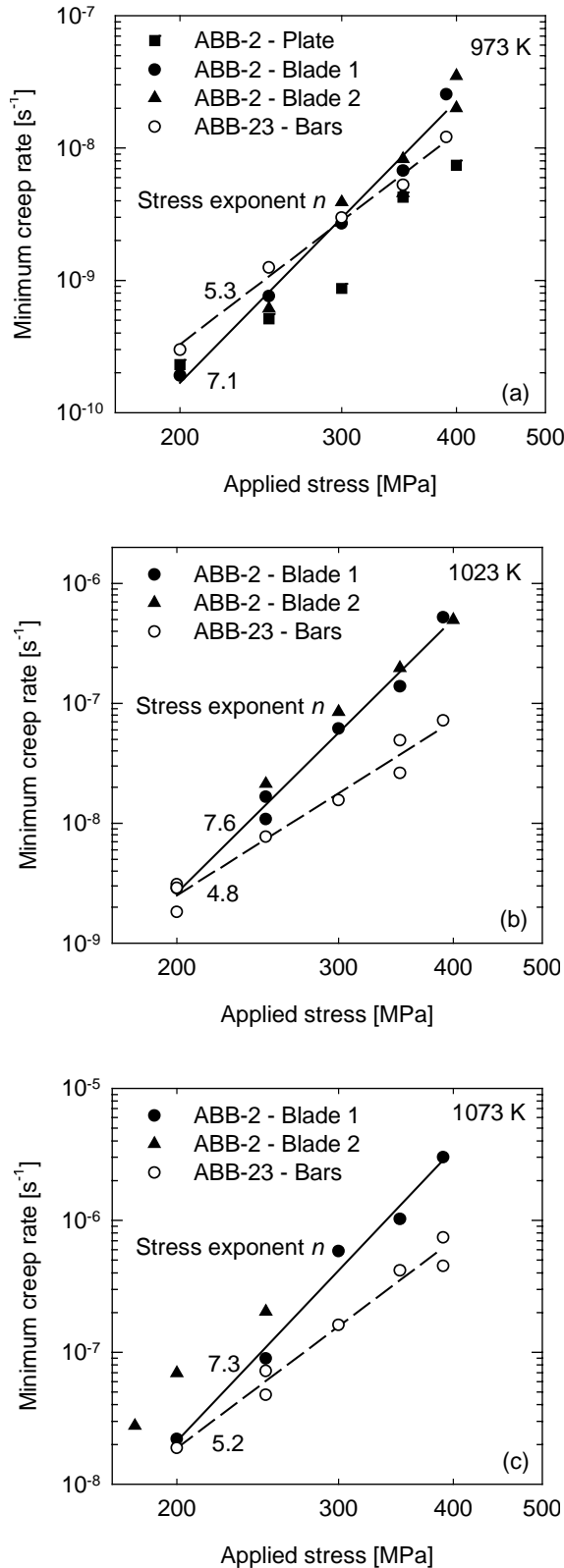


Fig. 4. Variation of the minimum creep rate with the applied stress for the ABB-2 and ABB-23 alloys: (a) 973 K, (b) 1023 K, (c) 1073 K. The stress exponents, test temperatures and type of tested components are indicated in the figures.

about 10 at high stresses reported by Appel and Wagner [29] for various TiAl-based alloys. Relatively large scatter of the measured minimum creep rates among the cast ABB-2 components indicates lower reproducibility of the applied investment casting technology and heat treatments. In spite of the large scatter of minimum creep rates, all minimum creep rates measured for the ABB-2 alloy at temperatures of 1023 and 1073 K and applied stresses larger than 200 MPa are higher than those measured for the ABB-23 alloy. This difference increases with increasing applied load.

The stress-minimum creep rate-temperature data were also fitted to the Bailey-Norton power law expression

$$\dot{\epsilon}_{\min} = A' \sigma^n \exp\left(-\frac{Q_a}{RT}\right), \quad (2)$$

where  $A'$  is a constant,  $Q_a$  is the apparent activation energy for creep,  $R$  is the universal gas constant and  $T$  is the absolute temperature. The apparent activation energy for creep  $Q_a$  is calculated according to Eq. (2) in the form

$$Q_a = \left[ \frac{\partial \ln \dot{\epsilon}_{\min}}{\partial (1/RT)} \right]_{\sigma=\text{const}}. \quad (3)$$

The apparent activation energy for creep calculated for five different applied stresses at three different temperatures is 427 and 355 kJ/mol for the alloy ABB-2 and ABB-23, respectively. These values are higher than those of 250–295 kJ/mol determined for self-diffusion of Ti in TiAl [30]. On the other hand, the activation energy determined for creep of the ABB-23 alloy is comparable with a value of 358 kJ/mol reported for self-diffusion of Al in TiAl [30]. The measured activation energies for creep fall into the interval ranging from 230 to 430 kJ/mol reported for the creep of various TiAl-based alloys [29]. Figure 5 shows the minimum creep rate normalized by an exponential term including the apparent activation energy for creep, the absolute temperature and the universal gas constant as a function of the applied stress. From this figure, it is obvious that all creep data over the studied temperatures and applied stresses cluster around straight lines. Regression analysis of the creep data yields an equation for the minimum creep rate of the ABB-2 alloy in the form

$$\dot{\epsilon}_{\min} = 1.11 \times 10^{-4} \sigma^{7.3} \exp\left(-\frac{427\,000 \text{ J/mol}}{RT}\right) \quad (4)$$

and for the ABB-23 alloy in the form

$$\dot{\epsilon}_{\min} = 5.48 \times 10^{-3} \sigma^{5.1} \exp\left(-\frac{355\,000 \text{ J/mol}}{RT}\right). \quad (5)$$

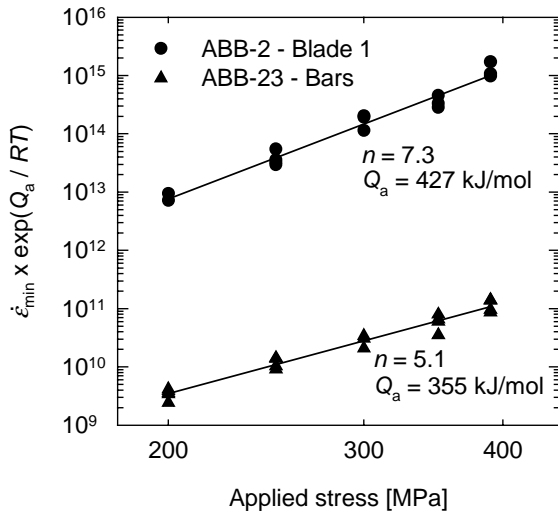


Fig. 5. Minimum creep rate normalized by the apparent activation energy for creep  $Q_a$ , the universal gas constant and the absolute temperature as a function of the applied stress. The type of tested components is indicated in the figure.

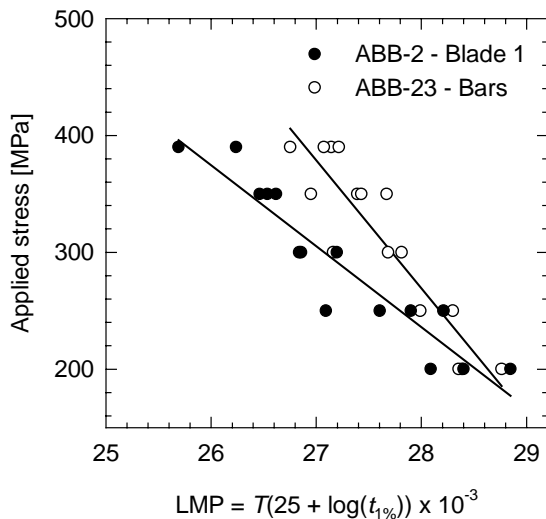


Fig. 6. Dependence of applied stress on the time to 1% creep deformation in the form of Larson-Miller graph. The type of tested components is indicated in the figure.

The correlation coefficients of these fits  $r^2$  are better than 0.96.

For rotating components like turbine blades, the maximum overall creep strain depends on the engine tolerance and is usually less than 1 %. From this point of view, the time to 1% creep deformation is of large interest. Figure 6 summarizes the dependence of the applied stress on the time to 1% creep deformation in the form of Larson-Miller parameter  $LMP = T(C + \log t_{1\%})$ , where  $C$  is a constant and  $t_{1\%}$  is the time to 1% creep deformation. The  $LMP$  is calculated

assuming a constant of  $C = 25$  and taking the measured time to 1% creep strain. The comparison of the creep data shows that the creep specimens prepared from the ABB-2 alloy have inferior 1% creep strain resistance than those prepared from the ABB-23 alloy but this difference decreases with decreasing applied stress. Superior creep resistance of the ABB-23 alloy can be attributed to better thermal stability of lamellar  $\alpha_2/\gamma$  regions when compared to that of the ABB-2 alloy [31].

### 3.3. Microstructure after creep

Microstructural observations of the crept specimens revealed that the initial microstructure of the ABB-2 and ABB-23 alloys is unstable. In the lamellar and feathery regions, the  $\alpha_2$ -phase transforms to the  $\gamma$  phase, B2 particles and fine  $Ti_5Si_3$  precipitates. The main microstructural change observed in the  $\gamma$ -rich region was precipitation of fine  $Ti_5Si_3$  particles. The applied stresses accelerate the coarsening kinetics of needle-like B2 particles [32]. The driving forces for such microstructural changes arise from changes of the phase equilibria. As proposed recently by Gil et al. [23] and Muñoz-Morris et al. [24] for the ABB-2 and ABB-23 alloys, the initial  $\gamma + \alpha_2 + B2$  microstructure formed during thermal treatments is inherently unstable and transforms to a stable  $\gamma + B2$  during ageing in the temperature range from 1173 to 1273 K. However, full transformation of the  $\alpha_2$  phase into the  $\gamma$  and B2 phases was not observed in this study. Such relatively good structural stability of the studied alloys can be explained by stabilizing effect of W, which shows strong partitioning into the  $\beta$  phase from the  $\alpha$  and  $\gamma$  phases and stabilizes also  $\alpha_2$  lamellae in the  $\gamma$  matrix. During ageing relatively large compositional changes of coexisting metastable phases must occur by diffusion of W to dissolve completely  $\alpha_2$  phase and to achieve equilibrium volume fraction of B2 and  $\gamma$  phases at given temperature. However, the diffusivity of W is known to be very slow at the temperatures of engineering interest [33], which explains stabilization of  $\alpha_2$  phase in the microstructure.

Superior creep resistance of the ABB-23 alloy when compared to that of the ABB-2 is in a very good agreement with our previous comparative study on the microstructure stability of the studied alloys [31]. Since these alloys differ also in the content of aluminium (1 at.%), better lamellar structure stability of the ABB-23 alloy can be only partially attributed to a positive effect of boron. Besides the grain refinement, boron refines the lamellar structure ( $\lambda = 530$  nm) of the ABB-23 alloy when compared to that of the ABB-2 ( $\lambda = 645$  nm). However, the mechanisms, how the minor boron additions affect the stability of  $\alpha_2/\gamma$  lamellar structure in tungsten containing alloys with the same aluminium content, are still unknown.

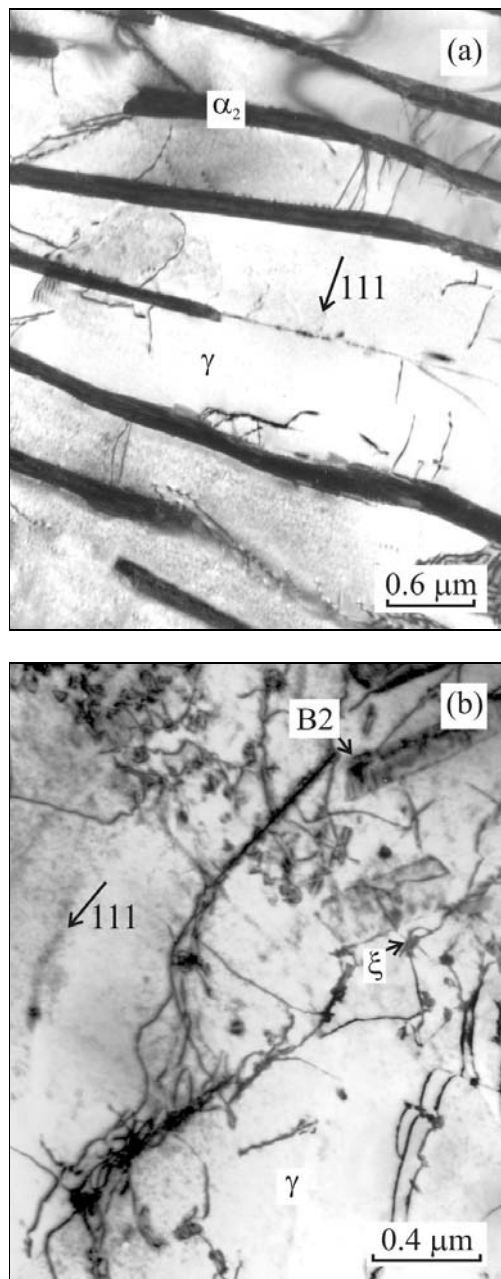


Fig. 7. TEM micrographs showing the deformation microstructures in the ABB-2 alloy after creep test at 973 K/200 MPa for 7300 h to a creep strain of 1.3 %: (a) lamellar region – zone axis near  $[1\bar{1}0]$  and  $g$  vector (111), (b)  $\gamma$ -rich region – zone axis near  $[1\bar{1}0]$  and  $g$  vector (111).  $\xi$  –  $\text{Ti}_5\text{Si}_3$  precipitates.

Zhou et al. [22] assumed that B segregates at the lamellar  $\alpha_2/\gamma$  and  $\gamma/\gamma$  interfaces and improves stability of lamellar structure by: (i) decreasing number of faults in the lamellar structure and (ii) formation of boride precipitates at the interfaces, which retards initial critical processes leading to lamellar instabilities. However, previous studies of Larson et al. [34, 35] showed no appreciable evidence of boron segregation

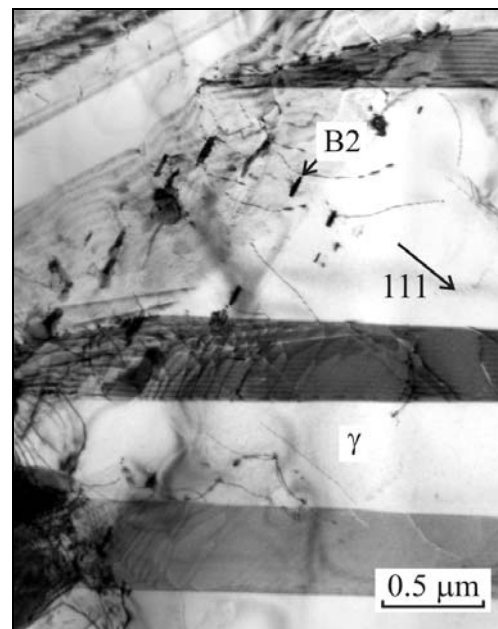


Fig. 8. TEM micrograph showing deformation twins in the ABB-2 alloy after creep testing at 1023 K/200 MPa for 25667 h to a creep strain of 6.7 %. Zone axis near  $[1\bar{1}0]$  and  $g$  vector (111).

or boride precipitation to lamellar  $\gamma/\gamma$  and  $\alpha_2/\gamma$  interfaces in Ti-47Al-2Cr-2Nb-0.2W-0.15B (in at.%) alloy. Since the solubility of boron in the  $\gamma$  and  $\alpha_2$  phases is 0.011 and 0.003 at.%, respectively, boron mainly concentrates in the boride particles ( $\text{TiB}_2$  and  $\text{TiB}$ ) [34]. Li and Cao [36] showed that minor boron addition suppresses the formation of metastable feathery and Widmanstätten microstructure during heat treatments, which improves the thermal stability of the lamellar structure and prolongs the creep rupture life. Similar effect of B on the microstructure and creep resistance is also observed in the present work.

Microstructural observations revealed that the creep of the specimens to strains lower than about 1.5 % is dominated by  $1/2 \langle 110 \rangle$  type of ordinary dislocations in the  $\gamma$  matrix. The deformation is inhomogeneous with smaller dislocation densities in the thinner  $\gamma$  lamellae and significantly larger densities in the thicker  $\gamma$  lamellae, as seen in Fig. 7a. During long-term creep testing precipitation of fine  $\text{Ti}_5\text{Si}_3$  particles in the  $\gamma$  matrix was observed. These precipitates act as effective pinning points for ordinary dislocations, as seen in Fig. 7b. Clusters of coarse  $\text{Ti}_5\text{Si}_3$  particles also act as effective obstacles to dislocation motion so that dislocations are piled-up at the  $\gamma$  matrix/particle interfaces. The dislocations in the  $\gamma$  matrix tend to be elongated in the screw orientation and appear to be frequently pinned along their lengths. The dislocation segments form local cusps along the length of the dislocations. Such cusps are frequently associated with

the tall jogs on the screw segments of dislocations. The dislocation segments bowing between the jogs lie on parallel  $\{111\}$  planes and the jogs themselves lie on a cross slip plane. As shown by Appel [37], the jogs move by climb under the combined action of thermo-mechanical stresses and osmotic climb forces arising from the chemical potential of the excess of vacancies. The dislocation glide at intermediate and high applied stresses was suggested to be controlled by non-conservative dragging of such jogs along the length of screw dislocations [38]. As revealed by TEM observations of the crept specimens and stress reduction experiments [27, 28], creep of the ABB-2 and ABB-23 alloys at strains lower than 1.5 % is controlled by non-conservative motion of dislocations and contribution of deformation twinning is of a minor importance. Figure 8 shows formation of deformation twins at creep strains higher than 1.5 %. Contribution of such deformation twinning to the overall creep strain increases with increasing strain [39].

#### 4. Conclusions

The investigation of creep properties of cast Ti-46Al-2W-0.5Si and Ti-45Al-2W-0.6Si-0.7B (in at.%) alloys designated as ABB-2 and ABB-23, respectively, suggests the following conclusions:

1. Creep curves of both studied alloys show primary creep stage that is directly followed by a tertiary creep. Minimum creep rate is found to depend strongly on the applied stress and temperature. The stress exponents are determined to be 7.3 and 5.1 and apparent activation energies for creep are calculated to be 427 and 355 kJ/mol for the ABB-2 and ABB-23 alloy, respectively.

2. The initial microstructure of both alloys is unstable during creep in the temperature range 973–1073 K. Transformation of the  $\alpha_2$ (Ti<sub>3</sub>Al)-phase to the  $\gamma$ (TiAl)-phase, needle-like B2 particles and fine Ti<sub>5</sub>Si<sub>3</sub> precipitates is observed. However, this process is very slow at temperatures of engineering interest and continuous  $\alpha_2$  lamellae are preserved in the microstructure after long-term creep testing.

3. Minimum creep rates measured for the ABB-23 alloy at temperatures of 1023 and 1073 K and applied stresses higher than 200 MPa are lower than those measured for the ABB-2 alloy. The ABB-23 alloy has superior 1% creep strain resistance than that of the ABB-2 but this difference decreases with decreasing applied stress. Superior creep resistance of the ABB-23 alloy, when compared to that of the ABB-2, can be attributed to a better thermal stability of lamellar structure of the boron doped alloy.

4. Deformation microstructures at creep strains lower than 1.5 % are dominated by ordinary dislocations in the  $\gamma$  matrix. Strong interaction of dislo-

cations with fine precipitates is observed. The kinetics of creep deformation is controlled by non-conservative motion of ordinary dislocations at low creep strains.

#### Acknowledgements

The author gratefully acknowledges the financial support of the Slovak Grant Agency for Science under the contract VEGA 2/4166/24. He also expresses his thanks to Dr. M. Nazmy from ALSTOM Ltd for providing the experimental material.

#### References

- [1] DIMIDUK, D. M.: Mater. Sci. Eng. A, 263, 1999, p. 281.
- [2] BARTOLOTTA, P. A.—KRAUSE, D. L.: In: Gamma Titanium Aluminides 1999. Eds.: Kim, Y. W., Dimiduk, D. D., Loretto, M. H. Warrendale, PA, TMS 1999, p. 3.
- [3] RUGG, D.: In: Gamma Titanium Aluminides 1999. Eds.: Kim, Y. W., Dimiduk, D. D., Loretto, M. H. Warrendale, PA, TMS 1999, p. 11.
- [4] NAZMY, M.—LUPINC, V.: In: Materials for Advanced Power Engineering 2002. Eds.: Lecomte-Beckers, J., Carton, J. M., Schubert, F., Ennis, P. J. Vol. 21. Forschungszentrum Jülich GmbH, Part I, 2002, p. 43.
- [5] SMARSLY, W.—BAUR, F.—GLITZ, G.—CLEMENS, H.—KHAN, T.—THOMAS, M.: In: Structural Intermetallics 2001. Eds.: Hemker, K. J., Dimiduk, D. M., Clemens, H., Darolia, R., Inui, H., Larsen, J. M., Sikka, V. K., Thomas, M., Whittenberger, J. D. Warrendale, PA, TMS 2001, p. 25.
- [6] TETSUI, T.: Mater. Sci. Eng. A, 329–331, 2002, p. 582.
- [7] VOJTĚCH, D.—ČÍŽOVÁ, H.—MAIXNER, J.: Kovove Mater., 43, 2005, p. 317.
- [8] LUKÁŠ, P.—ČADEK, J.—KUNZ, L.—SVOBODA, M.—KLUSÁK, J.: Kovove Mater., 43, 2005, p. 5.
- [9] MALDINI, M.—LUPINC, V.—ANGELLA, G.: Kovove Mater., 42, 2004, p. 283.
- [10] MALDINI, M.—LUPINC, V.—ANGELLA, G.: Kovove Mater., 42, 2004, p. 21.
- [11] LAPIN, J.: Kovove Mater., 40, 2002, p. 209.
- [12] VAŇO, A.—PELACHOVÁ, T.: Kovove Mater., 42, 2004, p. 121.
- [13] LAPIN, J.—BAJANA, O.: Kovove Mater., 43, 2005, p. 169.
- [14] FLORIAN, M.: Kovove Mater., 41, 2003, p. 73.
- [15] PRAHL, J.—HAUŠILD, P.—KARLÍK, M.—CRENN, J. F.: Kovove Mater., 43, 2005, p. 134.
- [16] KRATOCHVÍL, P.—HANUS, P.—HAKL, J.—VLAŠÁK, T.: Kovove Mater., 42, 2004, p. 73.
- [17] HAUŠILD, P.—KARLÍK, M.—NEDBAL, I.—PRAHL, J.: Kovove Mater., 42, 2004, p. 156.
- [18] HARDING, R. A.: Kovove Mater., 42, 2004, p. 225.
- [19] NAZMY, M.—STAUBLI, M.: U.S. Pat.#5,207,982 and European Pat.#45505 BI.

- [20] HU, D.: *Intermetallics*, 19, 2001, p. 1037.
- [21] KIM, Y. W.: *Acta Metall. Mater.*, 40, 1992, p. 1121.
- [22] ZHOU, L. Z.—LUPINC, V.—GUO, J. T.: *Mater. Sci. Eng. A*, 354, 2003, p. 97.
- [23] GIL, I.—MUÑOZ-MORRIS, M. A.—MORRIS, D. G.: *Intermetallics*, 9, 2001, p. 373.
- [24] MUÑOZ-MORRIS, M. A.—GIL, I.—MORRIS, D. G.: *Intermetallics*, 13, 2005, p. 929.
- [25] MUÑOZ-MORRIS, M. A.—FERNÁNDEZ, I. G.—MORRIS, D. G.: *Scripta Mater.*, 46, 2002, p. 617.
- [26] LAPIN, J.—PELACHOVÁ, T.: *Kovove Mater.*, 42, 2004, p. 143.
- [27] LAPIN, J.: *Kovove Mater.*, 43, 2005, p. 81.
- [28] LAPIN, J.: *Scripta Mater.*, 50, 2004, p. 261.
- [29] APPEL, F.—WAGNER, R.: *Mater. Sci. Eng. R*, 22, 1998, p. 187.
- [30] MISHIN, Y.—HERZIG, C.: *Acta Mater.*, 48, 2000, p. 589.
- [31] LAPIN, J.—PELACHOVÁ, T.: *Intermetallics*, 14, 2006 (in press).
- [32] LAPIN, J.—NAZMY, M.—STAUBLI, M.: In: *Proceeding of the International Symposium on Integrative and Interdisciplinary Aspects of Intermetallics*. Eds.: Mills, M. J., Inui, H., Clemens, H. H., Fu, C. L. Vol. 842. *Mater. Res. Soc. Symp. Proc.*, 2005, p. 115.
- [33] KAINUMA, R.—FUJITA, Y.—MITSUI, H.—OHNUMA, I.—ISHIDA, K.: *Intermetallics*, 8, 2000, p. 55.
- [34] LARSON, D. J.—LIU, C. T.—MILLER, M. K.: *Intermetallics*, 5, 1997, p. 411.
- [35] LARSON, D. J.—LIU, C. T.—MILLER, M. K.: *Mater. Sci. Eng. A*, 239–240, 1997, p. 220.
- [36] LI, Z. X.—CAO, C. C.: *Intermetallics*, 13, 2005, p. 251.
- [37] APPEL, F.: *Intermetallics*, 9, 2001, p. 907.
- [38] KARTHIKEYAN, S.—VISWANATHAN, G. B.—GOUMA, P. I.—VIJAY, K.—VASUDEVAN, V. K.—KIM, Y. W.—MILLS, M. J.: *Mater. Sci. Eng. A*, 329–331, 2002, p. 621.
- [39] ORLOVÁ, A.—KUCHAŘOVÁ, K.—DLOUHÝ, A.: *Kovove Mater.*, 43, 2005, p. 55.